Anisotropic superconductivity and elongated vortices with unusual bound states in quasi-one-dimensional nickel-bismuth compounds

Wen-Lin Wang,[1] Yi-Min Zhang,[1] Yan-Feng Lv,[1] Hao Ding,[1] Lili Wang,[1,2] Wei Li,[1,2] Ke He,[1,2] Can-Li Song,[1,2,*] Xu-Cun Ma,[1,2,†] and Qi-Kun Xue[1,2,‡]

[1]*State Key Laboratory of Low-Dimensional Quantum Physics, Department of Physics, Tsinghua University, Beijing 100084, China*

[2]*Collaborative Innovation Center of Quantum Matter, Beijing 100084, China*

(Received 29 December 2017; revised manuscript received 18 April 2018; published 30 April 2018)

We report low-temperature scanning tunneling microscopy and spectroscopy studies of Ni-Bi films grown by molecular beam epitaxy. Highly anisotropic and twofold symmetric superconducting gaps are revealed in two distinct composites, Bi-rich $NiBi_3$ and near-equimolar Ni_xBi, both sharing quasi-one-dimensional crystal structure. We further reveal axially elongated vortices in both phases, but Caroli–de Gennes–Matricon states solely within the vortex cores of $NiBi_3$. Intriguingly, although the localized bound state splits energetically off at a finite distance ∼10 nm away from a vortex center along the minor axis of elliptic vortex, no splitting is found along the major axis. We attribute the elongated vortices and unusual vortex behaviors to the combined effects of twofold superconducting gap and Fermi velocity. The findings provide a comprehensive understanding of the electron pairing and vortex matter in quasi-one-dimensional superconductors.

DOI: 10.1103/PhysRevB.97.134524

I. INTRODUCTION

Superconductivity in reduced dimensionality has long been of interest in condensed-matter physics, particularly given that most superconductors with relatively higher transition temperature T_c, regardless of whether they are unconventional cuprates [1] and iron pnictides [2] or conventional MgB_2 [3], have quasi-two-dimensional (2D) layered structure. It becomes more interesting insofar after the interface superconductivity with an unexpectedly high $T_c > 65$ K in single-layer FeSe films grown on $SrTiO_3$ was recently discovered [4]. In the last three decades, much has been learned about the novel pairing phenomena and exotic phenomena in quasi-2D superconductors. As the dimensionality is further reduced to the quasi-one-dimensional (1D) case, however, how the electrons would pair up and behave is little explored. This has been hindered primarily by the rare occurrence of superconductivity in quasi-1D electron systems. Thus far, only a few quasi-1D compounds, such as the Bechgaard salts $(TMTSF)_2X$ ($X = PF_6$, ClO_4) [5,6], $Li_{0.9}Mo_6O_{17}$ [7], $Ta_4Pd_3Te_{16}$ [8], and the recently discovered chromium pnictides $A_2Cr_3As_3$ (A = K, Rb, and Cs) [9], are found to be superconducting. A comprehensive understanding of electron pairing and vortex states in quasi-1D systems is currently lacking.

Recently, owing to its availability of cleavage plane, the quasi-1D $Ta_4Pd_3Te_{16}$ superconductor with an anisotropy of about 2.5 [10] was investigated on the atomic scale by means of scanning tunneling microscopy (STM) [11,12], but leading to several obvious controversies. First, the measured superconducting energy gaps were distinctively accounted for by isotropic [11] or anisotropic [12] electron pair functions. Second, although the elongated magnetic vortices were consistently observed, there exists great ambiguity as regards the vortex core states. Neither the observed double-peak feature around the vortex centers [11] nor the nonsplit zero-bias conductance (ZBC) peaks when away from the vortex center [12] appears contradictory with previous reports, in which the ZBC peaks caused by vortex bound states [13] often split off energetically starting from the vortex center in both anisotropic [14,15] and isotropic superconductors [16]. A concern over the electron pairing and vortex states has therefore emerged in quasi-1D superconductors. In this study, we reveal the anisotropic superconductivity and unusual vortex states in two quasi-1D Ni-Bi films grown by molecular beam epitaxy (MBE), which exhibits a comparable anisotropy with $Ta_4Pd_3Te_{16}$ [17], and provide a detailed microscopic view of quasi-1D superconductors.

II. EXPERIMENT

Our experiments were carried out in an ultrahigh vacuum cryogenic STM system (Unisoku), which is connected with a MBE chamber for *in situ* sample preparation. The base pressure of both chambers is better than 1.0×10^{-10} Torr. Nb-doped (∼0.05 wt %) $SrTiO_3$(001) substrates were cleaned by annealing at 1250 °C for 20 min. High-quality Ni-Bi epitaxial films were grown on $SrTiO_3$(001) at ∼ 280 °C–300 °C by thermal evaporation of high-purity Ni (99.994%) and Bi (99.997%) sources from two standard Knudsen cells. Details of the sample preparation are given in the Appendix. The temperatures of Ni and Bi sources were respectively set at 1200 °C and 495 °C, resulting in a growth rate of approximately 0.1 nm per minute. The optimal growth was achieved under Bi-rich condition, bearing a similarity to that for β-Bi_2Pd films [18]. Polycrystalline PtIr tips were cleaned by electron beam

*clsong07@mail.tsinghua.edu.cn
†xucunma@mail.tsinghua.edu.cn
‡qkxue@mail.tsinghua.edu.cn

TABLE I. Lattice parameters and structure of Ni-Bi phases.

	NiBi	Ni_xBi	$NiBi_3$
a (Å)	4.08	14.12	8.88
b (Å)	4.08	8.15	4.11
c (Å)	5.36	5.32	11.48
Space group	$P63/mmc$	$F12/m1$	$Pnma$
Structure	Hexagonal	Pseudo-orthorhombic	Orthorhombic

heating and calibrated prior to data collection at 0.4 K, unless otherwise specified. Tunneling conductance spectra and ZBC maps were measured by means of standard lock-in technique with a small bias modulation of 0.1 mV at 913 Hz.

III. RESULTS

A. Surface structure

Based on their mole ratio, the alloys of Ni and Bi can be crystallized into three distinct phases [19], with the crystal structures and lattice parameters summarized in Table I. The typical STM topographies of the three Ni-Bi phases, which can coexist on the as-grown films, are shown in Figs. 1(a)–1(c). Illustrated in Fig. 1(a) is the first stoichiometric NiAs-type NiBi phase with the space group $P63/mmc$ [Fig. 1(d)], which presents a hexagonal supercell. The adjacent bright spheres are spaced 7.2 ± 0.2 Å apart, consistent with a reconstructed NiBi(0001)-$(\sqrt{3} \times \sqrt{3})R30^\circ$ surface.

As the Ni/Bi ratio slightly departs from unity, however, more specialized studies have previously found pseudo-orthorhombic Ni-Bi superstructure with a space group of $F12/m1$ [20,21], in which displaced and occupational modulations of Bi and Ni atoms lead to quasi-1D structure along the b axis. This near-equimolar Ni_xBi phase, as represented in Fig. 1(b), actually exhibits the expected in-plane lattice parameters: $a = 14.12$ Å, $b = 8.15$ Å [Fig. 1(e)]. Note that lattice discontinuities are always found to run along the b axis [Fig. 1(b)] and mainly originate from the off-stoichiometry created Ni/Bi vacancies. These vacancies appear beneficial in that one can easily tell the atoms along the 1D chain apart and measure the lattice parameter of $b = 8.15$ Å.

In Fig. 1(c), we show the third phase that appears predominantly at a lower growth temperature of 280 °C. The in-plane lattice constants are measured as $a = 8.17$ Å and $b = 4.13$ Å from the inserted high-resolution STM image in Fig. 1(c), which matches with the stoichiometric $NiBi_3$ phase [17,22–26]. The experimental lattice constants for all three Ni-Bi phases are further confirmed by fast Fourier transform (FFT) images of the three Ni-Bi species [Figs. 1(g)–1(i)], with the white arrows indicating the 2D reciprocal vectors a^* and b^*. By measuring the lengths of the a^* and b^* vectors, we can calculate the lattice parameters in real space based on their reciprocal relationship. For example, in Ni_xBi, we measured the lengths of a^* to be 0.71/nm, giving rise to a lattice constant $a = 14.08$ Å, close to the theoretical value of 14.12 Å. We can also obtain the lattice constants for the other two phases, which are in line with the values obtained directly from the real space and match well with the theoretical expectation. Notably, the

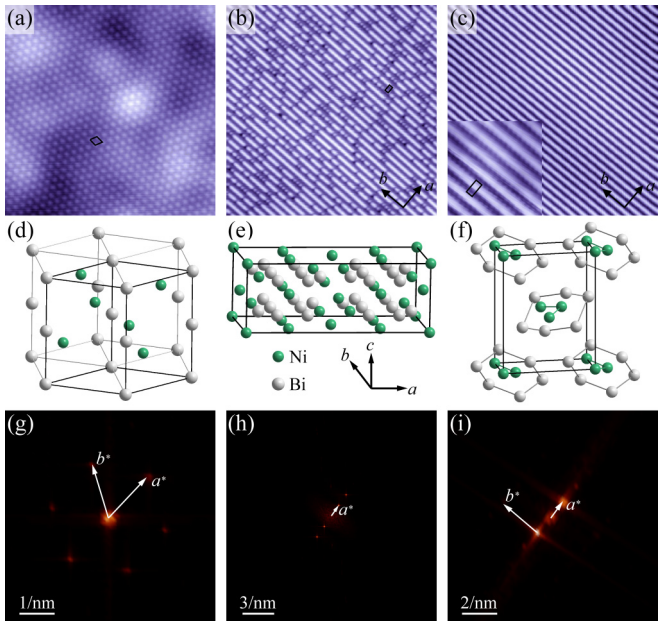

FIG. 1. (a)–(c) STM topographies of the as-grown Ni-Bi films presenting three distinct phases, i.e., (a) hexagonal NiBi ($V = 50$ mV, $I = 300$ pA, 20 nm × 20 nm), (b) pseudo-orthorhombic Ni_xBi ($V = 50$ mV, $I = 30$ pA, 45 nm × 45 nm), and (c) $NiBi_3$ ($V = 100$ mV, $I = 30$ pA, 26.7 nm × 26.7 nm). The white spots in (a) might originate from subsurface defects. The inset of (c) shows a higher-resolution STM image of $NiBi_3$ ($V = 100$ mV, $I = 30$ pA, 6 nm × 6 nm). The black rhombus and rectangles mark the unit cells of three Ni-Bi phases. (d)–(f) Schematic crystal structures of NiBi, Ni_xBi, and $NiBi_3$, with their unit cells marked by the thick black lines. The a, b, and c axes are oriented along the crystal directions of the two orthorhombic phases in (b) and (c). Note that the atom modulations in near-equimolar Ni_xBi are not displayed in (e). (g)–(i) FFT images of (a) hexagonal NiBi, (b) near-equimolar Ni_xBi, and (c) $NiBi_3$ films, respectively.

Bragg spots along the vector b^* are too weak to be resolved in Ni_xBi and one cannot tell the lattice constant b from the FFT image. Fortunately, we measure the lattice $b = 8.15$ Å from the real-space STM image, as discussed above.

Although some early studies indicated the coexistence of superconductivity and ferromagnetism in $NiBi_3$ [23–25], the recent work reveals that it might be amorphous Ni residuals that bear the responsibility for the magnetic signal [26]. As drawn in Fig. 1(f), the $NiBi_3$ could be best described as a packing of $NiBi_3$ rods. Within a single rod, the bonding is dominated by Ni-Ni and Ni-Bi interactions, while the Bi-Bi bonding appears significantly weak. Such a structural confinement provides another quasi-1D system [17,25], similar to the near-equimolar Ni_xBi.

B. Anistropic superconductivity

Scanning tunneling spectroscopy (STS) probes quasiparticle density of states (DOS) and provides key information of superconductivity. To eliminate possible disturbance from $SrTiO_3$ substrate, we here focus on thick Ni-Bi films with a thickness greater than 10 nm. Plotted in Fig. 2(a) are the large-energy-scale STS data at 0.4 K. Despite a sudden

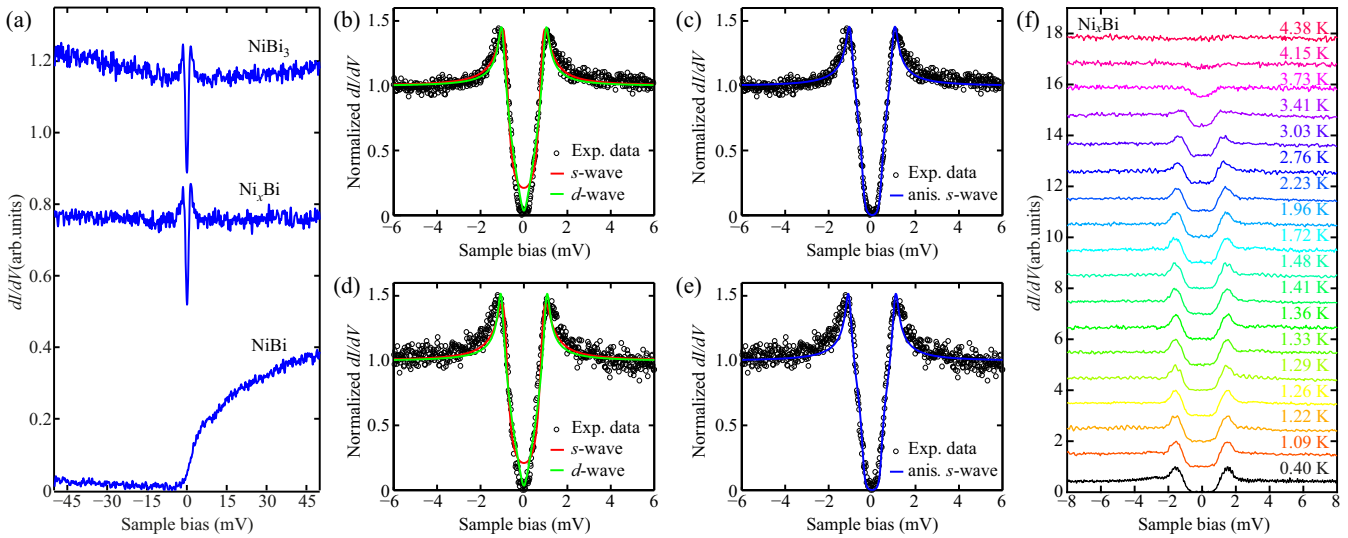

FIG. 2. (a) Differential conductance tunneling *dI/dV* spectra measured on Ni-Bi films. The curves on Ni_xBi and $NiBi_3$ have been vertically shifted for clarity. Set point: $V = 50$ mV, $I = 100$ pA. (b)–(e) Normalized *dI/dV* spectrum (black circles) on (b), (c) $NiBi_3$ and (d), (e) Ni_xBi. The colored lines show the best fits of experimental data to the Dynes model with *s*-wave, *d*-wave, and anisotropic *s*-wave gap functions. The normalization was performed by dividing the raw *dI/dV* spectra by their backgrounds, extracted from a linear fit to the conductance beyond the superconducting gaps. Set point: $V = 10$ mV, (b), (c) $I = 200$ pA, (d), (e) $I = 100$ pA. (f) Temperature-dependent *dI/dV* spectra of Ni_xBi films with a superconducting tip, revealing the disappearance of superconductivity at 4.38 K. The tunneling gap is stabilized at $V = 10$ mV and $I = 100$ pA.

DOS change around the Fermi level (E_F), the NiBi has no signature of superconductivity. In contrast, both the $NiBi_3$ and the Ni_xBi films exhibit symmetric gaps with respect to E_F. The gaps are suppressed and eventually vanish at elevated temperatures, indicating their origin from superconductivity. This thus provides two platforms to examine directly the electron pairing of quasi-1D superconductors by STS.

In order to gain insight into the pairing gap, we have collected and normalized the smaller-energy-scale *dI/dV* spectra, shown in Figs. 2(b)–2(e) as black empty symbols. We use tentatively the Dynes model with an effective energy broadening Γ [27], namely, $dI/dV \cong \mathrm{Re}[(E - i\Gamma)/\sqrt{(E - i\Gamma)^2 - \Delta^2}]$, to fit the experimental data with different categories of superconducting gaps, including isotropic *s*-wave gap, *d*-wave gap, and

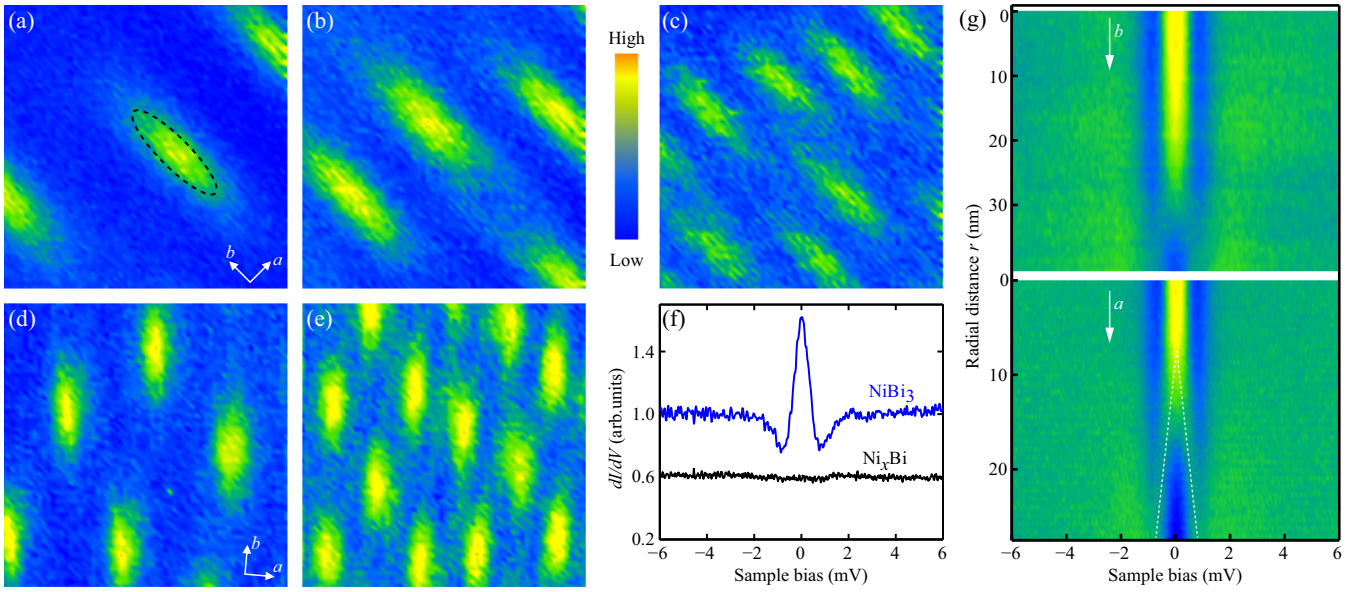

FIG. 3. (a)–(e) Zero-bias-conductance maps on (a)–(c) $NiBi_3$ (270 nm × 270 nm) and (d), (e) Ni_xBi (350 nm × 350 nm) films under various magnetic fields, revealing strongly axially elongated vortices. The black ellipse in (a) illustrates how unidirectional a single vortex is. The fields have magnitudes of 0.03 T in (a), 0.1 T in (b) and (d), and 0.2 T in (c) and (e), respectively. (f) STS curves on the center of vortex cores. (g) Dependences of *dI/dV* spectra of $NiBi_3$ on the radial distance *r* from a vortex center and crystallographic direction. The dotted lines mark the splitting of ZBC peaks along the *a* crystal axis. The tunneling gap is set at $V = 10$ mV, $I = 100$ pA except for (f), (g) $I = 200$ pA.

anisotropic s-wave gap. The results for optimized fits are color coded in Figs. 2(b)–2(e). It is evident that the isotropic s-wave scenario, marked by the red lines in Figs. 2(b) and 2(d), fails completely to track the low-energy DOS around E_F. Although the green solid lines with d-wave gaps can more reasonably follow the STS curves as a whole, they give rise to too sharp V-shaped features near the bottom, as compared to the STS data. We thus consider the scenario of anisotropic s-wave gap function to simulate the data. As justified below, the twofold symmetric gap $\Delta(\theta) = \Delta_1 + \Delta_2\cos(2\theta)$ rather than fourfold symmetric gap is favorable, although both functions lead to the same gap structure. As illustrated in Figs. 2(c) and 2(e), the anisotropic s-wave gaps interpret the experimental STS data quite nicely. This results in the gap function $\Delta_{NiBi_3}(\text{meV}) = 0.72 + 0.30\cos(2\theta)$ and $\Delta_{Ni_xBi}(\text{meV}) = 0.75 + 0.32\cos(2\theta)$ for $NiBi_3$ and Ni_xBi, respectively. The gap maximum Δ_{max} for $NiBi_3$ (Ni_xBi) is estimated to be 1.02 meV (1.07 meV), while the gap minimum Δ_{min} is 0.42 meV for both films. This suggests that despite large anisotropy there exists no node in the gap function.

The nodeless pairing is further confirmed by picking up a nanometer-sized Ni-Bi superconducting film on the end of the STM tip and performing the superconductor-insulator-superconductor tunneling spectrum, which allows for higher-energy resolution [28]. Figure 2(f) plots such STS spectra as a function of temperature, which were acquired on the Ni_xBi films. At the lower temperatures, the spectra reveal vanishing DOS over a finite energy range near E_F. This gives the convincing evidence of no nodes involved in the superconducting gap function of the Ni-Bi films investigated. At elevated temperatures, the superconducting gaps are progressively suppressed and completely vanish above 4.38 K. This suggests that the T_c of Ni_xBi studied lies between 4.15 and 4.38 K (~4.2 K), consistent with the reported value of 4.25 K [17]. We also measured the dI/dV spectrum on $NiBi_3$ and revealed the disappearance of superconducting gaps at an elevated temperature of 4.3 K, consistent with the expected $T_c = 4.06$ K [17]. Therefore, we estimate $T_c \sim 4.2$ K for Ni_xBi epitaxial films, although more careful experiments are needed to determine the T_c for the $NiBi_3$ films. Using the gap maxima Δ_{max}, we extract the reduced gap $2\Delta_{max}/k_BT_c$ is ~5.8 for Ni_xBi, suggesting strong-coupling superconductivity in Ni-Bi compounds. One might argue that multiband effects could be involved and a mixture of isotropic s-wave and d-wave gaps can also fit the STS data. However, a recent study from magnetoresistance measurements has revealed the dominance of only one band below 60 K in $NiBi_3$ [25]. The Ni-Bi films are thus most likely characteristic of an anisotropic single superconducting gap.

C. Magnetic vortices and unusual core states

Magnetic vortex imaging gains further insight into gap structure and vortex states of superconductors. Figures 3(a)–3(e) show the spatial ZBC maps under various magnetic fields, applied perpendicularly to the $NiBi_3$ [Figs. 3(a)–3(c)] and Ni_xBi [Figs. 3(d) and 3(e)] sample surfaces. The yellow stripelike regions have large ZBC due to the suppressed superconductivity and correspond to individual vortex cores, which are remarkably elongated along the b axis. The density of

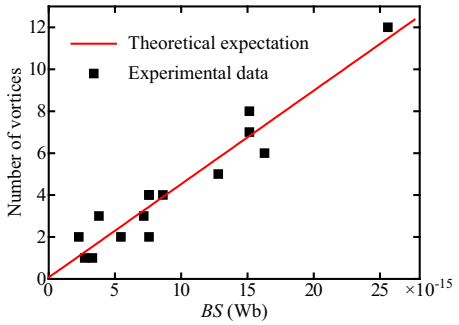

FIG. 4. Number of quantized magnetic vortices as a function of BS, with B and S representing the applied field and the area of ZBC maps holding the vortices, respectively. The red line corresponds to a linear fit of the experimental data.

vortices is found to increase linearly with the applied magnetic field [Fig. 4], as anticipated. The average flux per vortex is calculated to be $(2.09 \pm 0.16) \times 10^{-15}$ Wb, consistent with a single magnetic flux quantum, 2.07×10^{-15} Wb. Here the elongated vortex cores can be intuitively accounted for by the directional dependence of coherence lengths ξ. To calculate ξ, in Fig. 5(a) we extract the radial and directional dependence of ZBC in $NiBi_3$ and fit them by the Ginzburg-Landau expression for superconducting order parameter: $\text{ZBC}(r) = \text{ZBC}_\infty + (1 - \text{ZBC}_\infty)[1 - \exp(-r/\sqrt{2}\xi)]$ with ZBC_∞ representing the ZBC far away from the vortex core [29]. Figure 5(b) plots the angular dependence of ξ, from which we estimate the ratio ξ_b/ξ_a of as high as 3.9 in $NiBi_3$. This value appears larger than the anisotropy of Fermi velocity $v_{Fb}/v_{Fa} = 2.6$ [17]. Since ξ is cooperatively given by v_F and Δ via $\xi = \hbar v_F/\pi\Delta$, this supports the above-claimed anisotropy in Δ. Meanwhile, the pairing gap must be of twofold symmetry with gap minima along the b axis. Otherwise, the vortex core should be of fourfold or modulated fourfold symmetry. This thus rules out the possible involvement of the d-wave gap in quasi-1D $NiBi_3$. Such a rule might happen in Ni_xBi as well [blue symbols in Fig. 5(b)]. Here the ratio ξ_b/ξ_a is estimated to be about 3.8 and larger than the gap anisotropy of 2.55, suggesting that the Fermi velocity v_F is different along the a and b axes. This behaves analogous to that observed in $NiBi_3$. Moreover, the occurrence

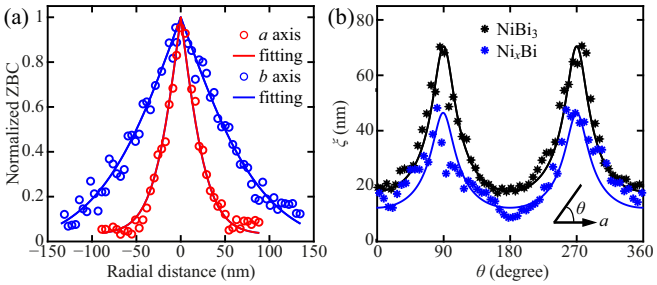

FIG. 5. (a), (b) Radial and directional dependence of normalized ZBC around a single magnetic vortex along the a (red spots) and b (blue spots) axes on $NiBi_3$ films, respectively. Solid lines show the theoretical fits of ZBC in $NiBi_3$. (b) Directional dependence of coherence length ξ in $NiBi_3$ (black symbols) and Ni_xBi (blue symbols) films. The angle θ is measured against the a axis. The solid lines are guides to the eyes.

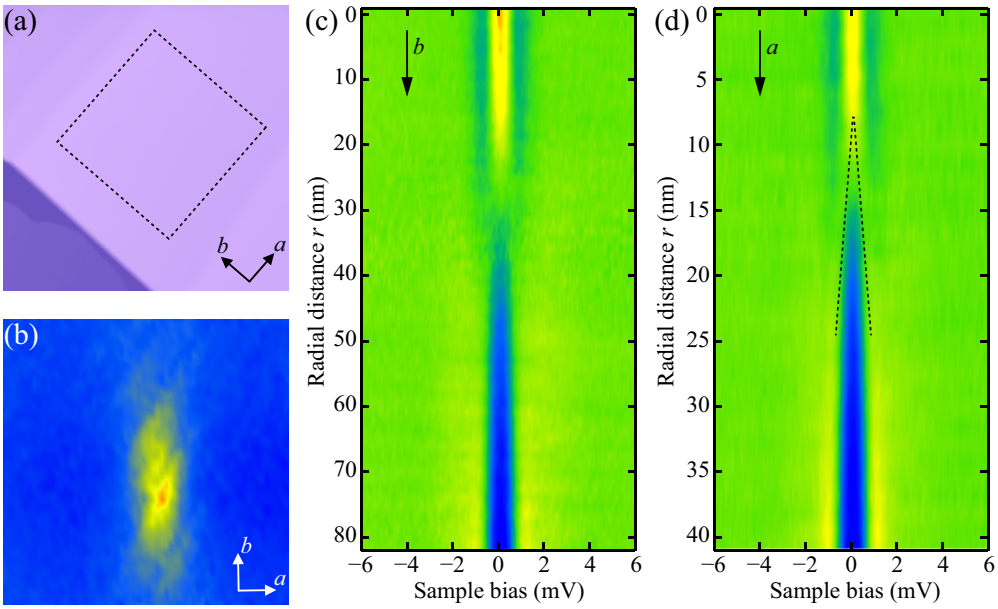

FIG. 6. (a) STM topographic image taken on another field of view of $NiBi_3$ films ($V = 3.5$ V, $I = 30$ pA, 300 nm × 300 nm). (b) Zero-bias-conductance map ($V = 10$ mV, $I = 100$ pA, 168 nm × 168 nm) taken on the square dashed-marked region in (a) at 0.1 T. (c), (d) Spatial and directional dependence of *dI/dV* spectra ($V = 10$ mV, $I = 200$ pA). The radial distance r is measured from the cortex center. The dotted lines in (d) mark the ZBC peak splitting along the a crystal axis, while no splitting is observed in (c).

of gap minimum along the b axis is consistent with the small DOS there, because the DOS scales inversely with v_F [30], which in our case appears larger along the b axis than that along the a axis. Notably the above results are subject to confirmation by the angular-dependent measurements of magnetoresistance and upper critical field H_{c2}. However, unfortunately, these parameters are not currently available, since the Ni-Bi samples studied here are only a few hundred nanometers in size and not large enough for a macroscopic investigation.

The most remarkable finding stands out by exploring the low-energy quasiparticle excitations in the vicinity of vortices. In Fig. 3(f), we show the STS data at the centers of vortices in $NiBi_3$ and Ni_xBi. Although the $NiBi_3$ holds a pronounced ZBC peak, no ZBC peak exists in Ni_xBi. Such a distinction might originate from the fact that off-stoichiometry-increased scattering significantly reduces the electron mean free path ℓ and pushes the Ni_xBi superconductor into the dirty region ($\ell < \xi$), where the constructive interference of repeated Andreev scatterings responsible for the ZBC peak can no longer be sustained within the vortex cores. Conversely, the presence of the ZBC peak means a longer ℓ than ξ (clean limit) in $NiBi_3$, which coincides with its high stoichiometry nature. Figure 3(g) shows the dependence of tunneling *dI/dV* spectra on the radial distance r away from a vortex center in $NiBi_3$. Quite strikingly, the ZBC peaks evolve quite differently along the a and b axes. Although the ZBC peak first decays and then begins to split into two symmetric branches in energy at a distance of $r \sim 10$ nm along the a axis (bottom panel), it exhibits no observable splitting along the b axis (upper panel). We emphasize that this unusual finding is inherent to superconducting $NiBi_3$, irrespective of the field of view we studied. This is well confirmed in Fig. 6. In a different field of view, we observe the identical behaviors of the vortex core states.

IV. DISCUSSIONS

The unprecedented variations of vortex-induced low-energy excitations differ substantially from the common Caroli–de Gennes–Matricon (CdGM) vortex bound states [13], which were often observed to split at sites quite close to the vortex center [14,31]. The retarded splitting of such peak around vortices was rarely found in the topological insulator $Bi_2Te_3/NbSe_2$ hybrid structure and interpreted as the involvement of Majorana zero modes [32,33]. The zero-energy Majorana mode comes into play together with the CdGM states and will delay the splitting of ZBC peaks around vortices. This might be possible for $NiBi_3$ because the Ni/Bi bilayer films, which inevitably contain $NiBi_3$ phase during the sample preparation [34], exhibit nontrivial superconducting states potentially harboring MZMs at vortices [35–37].

However, a more reasonable explanation might be that the observed vortex-core-state anomaly in Figs. 3(g) and 6 come solely from CdGM states in quasi-1D compounds with twofold superconducting properties. In the theoretical framework of CdGM states, the low-energy quasiparticle excitations around vortices consist of a series of discrete bound states, with the spacing of energy levels proportional to Δ and $1/v_F$ [38]. Along the b axis of quasi-1D $NiBi_3$, the smaller Δ and larger v_F conspire to lead to a small energy spacing of the bound states, which is difficult to be resolved due to the thermal smearing of 0.4 K in experiment. On the other hand, the energy spacing of bound states along the a axis (large Δ and small v_F) might be large enough to be discernible at a finite distance away from the vortex center [the bottom panel of Fig. 3(g)]. This scenario reasonably explains our findings above and can help understand the direction-dependent vortex core states in $Ta_4Pd_3Te_{16}$ as well [11,12]. Further experiment at a lower

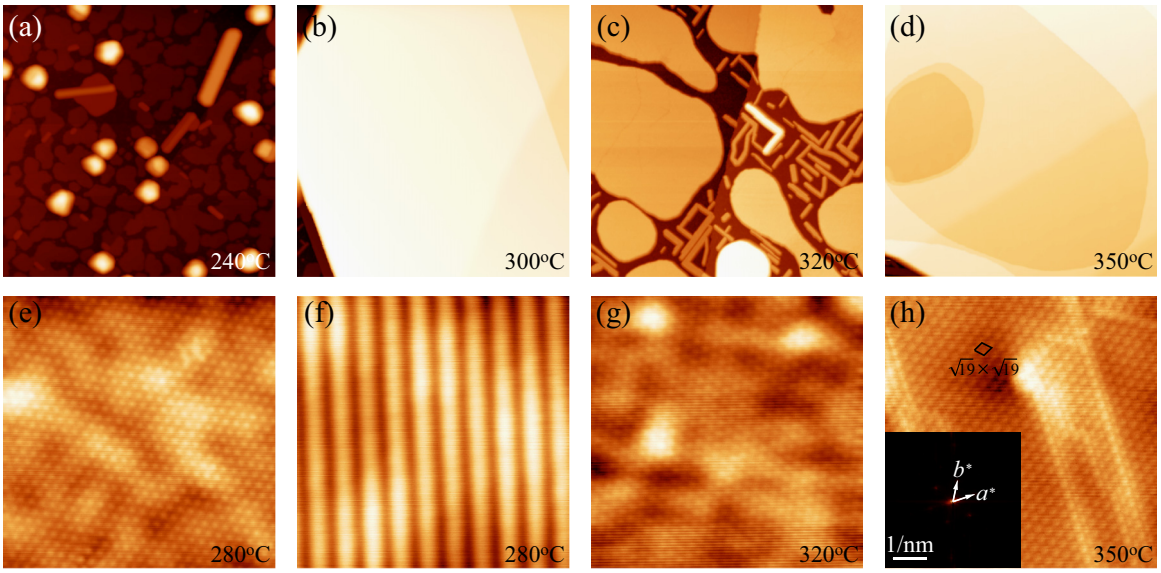

FIG. 7. (a)–(d) Morphology [$V = 3.5$ V, $I = 25$ pA, 500 nm × 500 nm, except for (d) 430 nm × 430 nm] and (e)–(h) zoom-in STM images of as-grown Ni-Bi films at various T_{sub} as indicated. Tunneling conditions and image size: (e) $V = 50$ mV, $I = 30$ pA, 18 nm × 18 nm; (f) $V = 50$ mV, $I = 30$ pA, 13 nm × 13 nm; (g) $V = 10$ mV, $I = 30$ pA, 18 nm × 18 nm; and (h) $V = 100$ mV, $I = 26$ pA, 45 nm × 45 nm.

temperature might help fully understand the mechanism behind the exotic vortex states observed in Fig. 3(g).

Finally we comment on vortex arrangement in quasi-1D superconductors. For isotropic s-wave superconductors, and when pinning is not quite effective, vortices are packed into a hexagonal lattice. On the other hand, a square vortex lattice with the sides along the directions of Δ or v_F minima, can be formed in superconductors with fourfold symmetric properties [30,39]. In quasi-1D compounds with twofold superconductivity state, however, the vortices are more distorted and could be roughly described by an oblique lattice [Figs. 3(c)–3(e)], although the $NiBi_3$ films are clean and have negligible vortex pinning. Such an oblique vortex lattice seems generic for superconductors with quasi-1D features, such as $YBa_2Cu_3O_{7-\delta}$ with ab-plane crystal anisotropy [40], FeSe with strong electronic nematicity [31], and $Ta_4Pd_3Te_{16}$ with a chainlike structure [11,12]. This might be due to the trade-off between the direction-dependent vortex-vortex interactions for elliptic vortices and the closest packing of vortices.

V. SUMMARY

In summary, our detailed STM/STS study of Ni-Bi epitaxial films has developed a comprehensive microscopic picture of quasi-1D superconductors. First, we have explicitly revealed by the conducting tunneling spectrum that quasi-1D superconductors are characteristic of twofold symmetric gap functions. Second, we have visualized elongated vortices, and more significantly revealed their (as well as the unusual CdGM vortex bound states) origin from the combined effects of twofold superconducting pairing and Fermi velocity in quasi-1D superconductors. Third, we have shown by spatially resolved spectroscopy that the CdGM bound states behave sharply different along the major and minor axes of elliptic vortices in quasi-1D superconductors. This allows for a reasonable explanation for the discrepancy of CdGM states in $Ta_4Pd_3Te_{16}$, and provides a complete microscopic view of vortex matter in quasi-1D superconductors.

ACKNOWLEDGMENTS

This work was financially supported by the Ministry of Science and Technology of China (2017YFA0304600, 2016YFA0301004) and National Science Foundation of China. C.L.S. acknowledges support from the National Thousand-Young-Talents Program and the Tsinghua University Initiative Scientific Research Program.

APPENDIX: SAMPLE PREPARATION

We prepared Ni-Bi epitaxial films on $SrTiO_3(001)$ substrate by using Bi-rich condition. A deficiency of the Bi element during the growth was found to result in polycrystalline Ni clusters. To grow crystalline Ni-Bi films, we have set the temperatures of Ni and Bi sources at 1200 °C and 490°C–500°C, respectively, which leads to a Bi/Ni flux ratio of around 1.5–2.2. A larger flux ratio of Bi/Ni leads to many unwanted small rods (most probably the excess Bi), in particular at a lower substrate temperature T_{sub} [Fig. 7(a)].

Figure 7 illustrates the STM morphologies and the corresponding atom resolution STM images of as-grown Ni-Bi films. The Ni-Bi compounds grow typically in a three-dimensional island mode. At the elevated substrate temperature $T_{sub} > 280$ °C [Figs. 7(b)–7(d)], the epitaxial Ni-Bi films with a lateral size of hundreds of nanometers could be found, which well satisfy our requirements for STM studies. A closer scrutiny of atomically resolved STM images reveal that although the stoichiometric NiBi, near-equimolar Ni_xBi, and Bi-rich $NiBi_3$ phases coexist in an intermediate substrate temperature $T_{sub} = 280$ °C–300 °C, a higher or lower T_{sub} leads to the exclusive hexagonal phase with various reconstructed surface structrues [Figs. 7(e), 7(g), and 7(h)]. For example, at $T_{sub} = 350$ °C, the frequently observed surface exhibits a

hexagonal superstructure with an extremely large period [Fig. 7(h)]. Based on the inserted FFT image in Fig. 7(h), the periodicity of the superstructure is estimated to be approximately 1.79 nm, matching excellently with a reconstructed NiBi(0001)-($\sqrt{19} \times \sqrt{19}$) surface. The absences of Bi-rich $NiBi_3$ and Ni_xBi phases at the higher T_{sub} are understandable, since the sticking coefficient of Bi on $SrTiO_3$ is significantly small at the higher T_{sub} [18], leading to a Bi-deficient environment in which only the Bi-poor hexagonal phase is formed. On the other hand, we hypothesize that the reason why no Bi-rich $NiBi_3$ and Ni_xBi phase exist at the lower T_{sub} might be their relatively higher formation energy than NiBi. In order to obtain the $NiBi_3$ and Ni_xBi phases, a sufficiently high T_{sub} ($> 280^{\circ}$) is thus required.

[1] J. G. Bednorz and K. A. Müller, Z. Phys. B **64**, 189 (1986).
[2] Y. Kamihara, T. Watanabe, M. Hirano, and H. Hosono, J. Am. Chem. Soc. **130**, 3296 (2008).
[3] J. Nagamatsu, N. Nakagawa, T. Muranaka, Y. Zenitani, and J. Akimitsu, Nature (London) **410**, 63 (2001).
[4] Q. Y. Wang, Z. Li, W. H. Zhang, Z. C. Zhang, J. S. Zhang, W. Li, H. Ding, Y. B. Ou, P. Deng, K. Chang, J. Wen, C. L. Song, K. He, J. F. Jia, S. H. Ji, Y. Y. Wang, L. L. Wang, X. Chen, X. C. Ma, and Q. K. Xue, Chin. Phys. Lett. **29**, 037402 (2012).
[5] D. Jérome, A. Mazaud, M. Ribault, and K. Bechgaard, J. Phys. Lett. **41**, L95 (1980).
[6] K. Bechgaard, K. Carneiro, M. Olsen, F. B. Rasmussen, and C. S. Jacobsen, Phys. Rev. Lett. **46**, 852 (1981).
[7] J. F. Mercure, A. F. Bangura, X. F. Xu, N. Wakeham, A. Carrington, P. Walmsley, M. Greenblatt, and N. E. Hussey, Phys. Rev. Lett. **108**, 187003 (2012).
[8] W. H. Jiao, Z. T. Tang, Y. L. Sun, Y. Liu, Q. Tao, C. M. Feng, Y. W. Zeng, Z. A. Xu, and G. H. Cao, J. Am. Chem. Soc. **136**, 1284 (2014).
[9] J. K. Bao, J. Y. Liu, C. W. Ma, Z. H. Meng, Z. T. Tang, Y. L. Sun, H. F. Zhai, H. Jiang, H. Bai, C. M. Feng, Z. A. Xu, and G. H. Cao, Phys. Rev. X **5**, 011013 (2015).
[10] J. Pan, W. H. Jiao, X. C. Hong, Z. Zhang, L. P. He, P. L. Cai, J. Zhang, G. H. Cao, and S. Y. Li, Phys. Rev. B **92**, 180505 (2015).
[11] Q. Fan, W. H. Zhang, X. Liu, Y. J. Yan, M. Q. Ren, M. Xia, H. Y. Chen, D. F. Xu, Z. R. Ye, W. H. Jiao, G. H. Cao, B. P. Xie, T. Zhang, and D. L. Feng, Phys. Rev. B **91**, 104506 (2015).
[12] Z. Y. Du, D. L. Fang, Z. Y. Wang, Y. F. Li, G. Du, H. Yang, X. Y. Zhu, and H. H. Wen, Sci. Rep. **5**, 9408 (2015).
[13] C. Caroli, P. G. De Gennes, and J. Matricon, Phys. Lett. **9**, 307 (1964).
[14] H. F. Hess, R. B. Robinson, and J. V. Waszczak, Phys. Rev. Lett. **64**, 2711 (1990).
[15] I. Guillamon, H. Suderow, F. Guinea, and S. Vieira, Phys. Rev. B **77**, 134505 (2008).
[16] I. Guillamón, H. Suderow, S. Vieira, L. Cario, P. Diener, and P. Rodière, Phys. Rev. Lett. **101**, 166407 (2008).
[17] Y. Fujimori, S. I. Kan, B. Shinozaki, and T. Kawaguti, J. Phys. Soc. Jpn. **69**, 3017 (2000).
[18] Y. F. Lv, W. L. Wang, Y. M. Zhang, H. Ding, W. Li, L. Wang, K. He, C. L. Song, X. C. Ma, and Q. K. Xue, Sci. Bull. **62**, 852 (2014).
[19] P. Nash, Bull. Bull. Alloy Phase Diagrams **6**, 345 (1985).
[20] M. Ruck, Z. Anorg. Allg. Chem. **625**, 2050 (1999).
[21] S. Lidin, V. Petricek, L. Stenberg, S. Furuseth, H. Fjellvåg, and A. K. Larsson, Solid State Sci. **2**, 353 (2000).
[22] J. Kumar, A. Kumar, A. Vajpayee, B. Gahtori, D. Sharma, P. Ahluwalia, S. Auluck, and V. Awana, Supercond. Sci. Technol. **24**, 085002 (2011).
[23] E. L. M. Piñeiro, B. L. R. Herrera, R. Escudero, and L. Bucio, Solid State Commun. **151**, 425 (2011).
[24] T. Herrmannsdörfer, R. Skrotzki, J. Wosnitza, D. Köhler, R. Boldt, and M. Ruck, Phys. Rev. B **83**, 140501 (2011).
[25] X. D. Zhu, H. C. Lei, C. Petrovic, and Y. H. Zhang, Phys. Rev. B **86**, 024527 (2012).
[26] B. Silva, R. F. Luccas, N. M. Nemes, J. Hanko, M. R. Osorio, P. Kulkarni, F. Mompean, M. García-Hernández, M. A. Ramos, S. Vieira, and H. Suderow, Phys. Rev. B **88**, 184508 (2013).
[27] R. C. Dynes, V. Narayanamurti, and J. P. Garno, Phys. Rev. Lett. **41**, 1509 (1978).
[28] S. H. Ji, T. Zhang, Y. S. Fu, X. Chen, X. C. Ma, J. Li, W. H. Duan, J. F. Jia, and Q. K. Xue, Phys. Rev. Lett. **100**, 226801 (2008).
[29] M. R. Eskildsen, M. Kugler, S. Tanaka, J. Jun, S. M. Kazakov, J. Karpinski, and O. Fischer, Phys. Rev. Lett. **89**, 187003 (2002).
[30] N. Nakai, P. Miranović, M. Ichioka, and K. Machida, Phys. Rev. Lett. **89**, 237004 (2002).
[31] C. L. Song, Y. L. Wang, P. Cheng, Y. P. Jiang, W. Li, T. Zhang, Z. Li, K. He, L. Wang, J. F. Jia, H. H. Hung, C. J. Wu, X. C. Ma, X. Chen, and Q. K. Xue, Science **332**, 1410 (2011).
[32] J. P. Xu, M. X. Wang, Z. L. Liu, J. F. Ge, X. J. Yang, C. H. Liu, Z. A. Xu, D. D. Guan, C. L. Gao, D. Qian, Y. Liu, Q. H. Wang, F. C. Zhang, Q. K. Xue, and J. F. Jia, Phys. Rev. Lett. **114**, 017001 (2015).
[33] T. Kawakami and X. Hu, Phys. Rev. Lett. **115**, 177001 (2015).
[34] V. Siva, K. Senapati, B. Satpati, S. Prusty, D. Avasthi, D. Kanjilal, and P. K. Sahoo, J. Appl. Phys. **117**, 083902 (2015).
[35] X. X. Gong, H. X. Zhou, P. C. Xu, D. Yue, K. Zhu, X. F. Jin, H. Tian, G. J. Zhao, and T. Y. Chen, Chin. Phys. Lett. **32**, 067402 (2015).
[36] J. H. Wang, X. X. Gong, G. Yang, Z. Z. Lyu, Y. Pang, G. T. Liu, Z. Q. Ji, J. Fan, X. N. Jing, C. L. Yang, F. M. Qu, X. F. Jin, and L. Lu, Phys. Rev. B **96**, 054519 (2017).
[37] X. X. Gong, M. Kargarian, A. Stern, D. Yue, H. X. Zhou, X. F. Jin, V. M. Galitski, V. M. Yakovenko, and J. Xia, Sci. Adv. **3**, e1602579 (2017).
[38] N. Hayashi, T. Isoshima, M. Ichioka, and K. Machida, Phys. Rev. Lett. **80**, 2921 (1998).
[39] H. Sakata, M. Oosawa, K. Matsuba, N. Nishida, H. Takeya, and K. Hirata, Phys. Rev. Lett. **84**, 1583 (2000).
[40] I. Maggio-Aprile, C. Renner, A. Erb, E. Walker, and O. Fischer, Phys. Rev. Lett. **75**, 2754 (1995).